Zn₂SiO₄/ZnO Core/Shell Coaxial Heterostructure Nanobelts Formed by an Epitaxial Growth

Baochang Cheng,*,† Xiaoming Yu,† Hongjuan Liu,† and Zhanguo Wang‡

Institute for Advanced Studying and School of Materials Science and Engineering, Nanchang University, Nanchang 330031, People's Republic of China, and Key Laboratory of Semiconductor Materials Science, Institute of Semiconductors, Chinese Academy of Science, Beijing 100083, People's Republic of China

Si-doped ZnO can be synthesized on the surface of the early grown Zn₂SiO₄ nanostructures and form core/shell coaxial heterostructure nanobelts with an epitaxial orientation relationship. A parallel interface with a periodicity array of edge dislocations and an inclined interface without dislocations can be formed. The visible green emission is predominant in PL spectra due to carrier localization by high density of deep traps from complexes of impurities and defects. Due to band tail localization induced by composition and defect fluctuation, and high density of free-carriers donated by doping, especially the further dissociation of excitons into free-carriers at high excitation intensity, the near-band-edge emission is dominated by the transition of free-electrons to free-holes, and furthermore, exhibits a significant excitation power-dependent red-shift characteristic. Due to the structure relaxation and the thermalization effects, carrier delocalization takes place in deep traps with increasing excitation density. As a result, the green emission passes through a maximum at $0.25I_0$ excitation intensity, and the ratio of the violet to green emission increases monotonously as the excitation laser power density increases. The violet and green emission of ZnO nanostructures can be well tuned by a moderate doping and a variation in the excitation density.

1. Introduction

As a wide direct band gap semiconductor, ZnO has been studied extensively for a long time due to its important application in optoelectronic devices such as UV light-emitting diodes and lasers, surface acoustic wave devices, and window material for display and solar cells.[1] Especially for one-dimensional nanostructured ZnO, it can be used as building blocks for fabricating nanolasers, field effect transistors and gas sensors, nanocantilevers, nanogenerators, and nanoresonators.[2] Therefore, much effort is being paid to in situ control of the structure, morphology, position, and composition of nanomaterials during the growth, and a diverse group of ZnO nanostructures has been widely grown.[3] To satisfy the different requirements in nanodevices, a number of approaches have been taken to modulate optical properties of ZnO nanostructures.

As is well-known, doping in semiconductors with selective elements offers an effective method to adjust their electrical, optical, and magnetic properties, which is crucial for their practical application. Recently, there have been intensive studies on the subject by doping exotic dopants or depositing multilayer structures to realize the above purpose.[4] Moreover, when impurities are mixed into the source materials and diffuse into nanostructures during the growth, not only can more ZnO complex structures be developed, but the electronic and optical properties of nanostructures can be improved.[5] Therefore, the growth and performance of ZnO nanomaterials can be manipulated by choosing appropriate conditions to influence the growth kinetics or thermodynamics,[6] Although masses of research have been done on ZnO doping, it still remains a challenge to achieve

efficient carrier density in 1D semiconductors.[7] Group IV elements have an indirect band gap and energy difference between indirect gap and direct gap, which leads to tuning the electronic structure around the band edge.[8] Here, we applied a vapor-transport-deposition method to synthesize Si-doped ZnO nanobelts and the results demonstrate that the introduction of Si can induce the formation of ZnO nanobelts by an epitaxial growth on the early growth Zn₂SiO₄ nanostructures and affect greatly the optical properties of the nanostructures.

2. Experimental Section

Synthesis. The samples were fabricated through a simple vapor deposition method. ZnS powder was placed at the middle of a ceramic tube and Si powder was located about 2 cm downstream from the ZnS source. The thermal evaporation process was carried out at 1200 °C in an Ar gas for 2 h. Subsequently, the sample was annealed at 800 °C in air atmosphere for 1 h to eliminate the influence of S element.

Characterization. The structure, morphology, and composition of the as-synthesized nanostructures were investigated by using X-ray diffraction (XRD; Phillip X'Pert PRO with Cu Kα radiation), field emission scanning electron microscopy (FE-SEM, FEI Siron200), transmission electron microscopy (TEM; JEOL JEM-2000FX, at 160 kV) equipped with energy-dispersive X-ray spectroscopy (EDS), and high-resolution TEM (HRTEM; JEOL JEM-2010, at 200 kV). Because the photoluminescence (PL) properties are sensitive to excitation energy, two types of excitation-light source have been applied to measure the optical properties of sample. The room temperature photoluminescence (PL) and PL excitation (PLE) spectra of the sample were recorded with use of a fluorescence spectrophotometer (Edinburgh FLS920) with a 450 W Xe lamp as a light source. The power-dependent room temperature micro-PL spectra were measured by the micro-PL system of a Confocal

* To whom correspondence should be addressed. Fax: +86-791-3969554. E-mail: bcheng@vip.sina.com.
† Nanchang University.
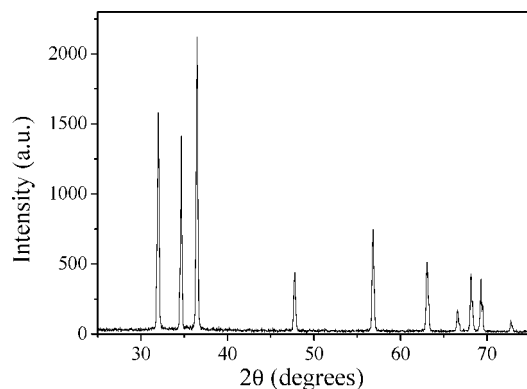‡ Institute of Semiconductors, Chinese Academy of Science.

Zn$_2$SiO$_4$/ZnO Core/Shell Coaxial Heterostructure Nanobelts

J. Phys. Chem. C, Vol. 112, No. 42, 2008 **16313**

Figure 1. A representative XRD pattern from a collection of nanostructures.
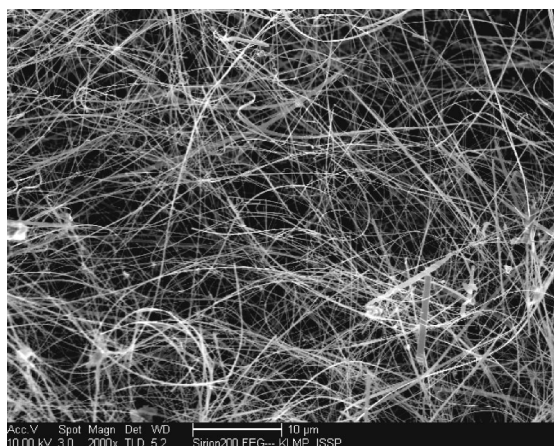

Figure 2. FE-SEM image of the as-grown nanostructure.

Laser Micro-Raman spectrometer (Jobin Yvon, LABRAM-HR), using a He−Cd laser with about 2mW output at 325 nm as an excitation light source. The incident light is focused on a spot of about 5 μm diameter by a microscopic objective and the corresponding maximum intensity of excitation light is about 20 kw/cm^2. For optical absorption measurement, the products were first ultrasonically dispersed in anhydrous ethanol, and then the measurement was performed with a Cary 5E UV−vis−NIR spectrophotometer at room temperature.

3. Results and Discussion

The XRD pattern of the as-synthesized nanostructure is shown in Figure 1. Only peaks corresponding to a hexagonal wurtzite structured ZnO are observed. No reflections attributable to other phases, such as zinc silicate, are observed in the product, indicating that other phases are present in negligible amounts. Figure 2 shows a typical distribution in the morphology for nanostructures by a FE-SEM. The image reveals that nanobelts are predominant in the sample, varying in width from several tens to hundreds of nanometers and thickness from several to several tens of nanometers.

As seen from bright-field images of TEM (Figure 3), the product presents a nanobelt-like morphology. Moreover, there is a great difference in contrast between the core and the two edges, showing a thin "dark" core and two "bright" edges along the axis of the nanobelts with smooth surfaces and sharp interfaces. This indicates the structure of the edges is different from that of the core, and the nanobelts with a core/shell coaxial heterostructure are formed. The selected area electron diffraction (SAED) pattern (Figure 3d), taken with the incident beam
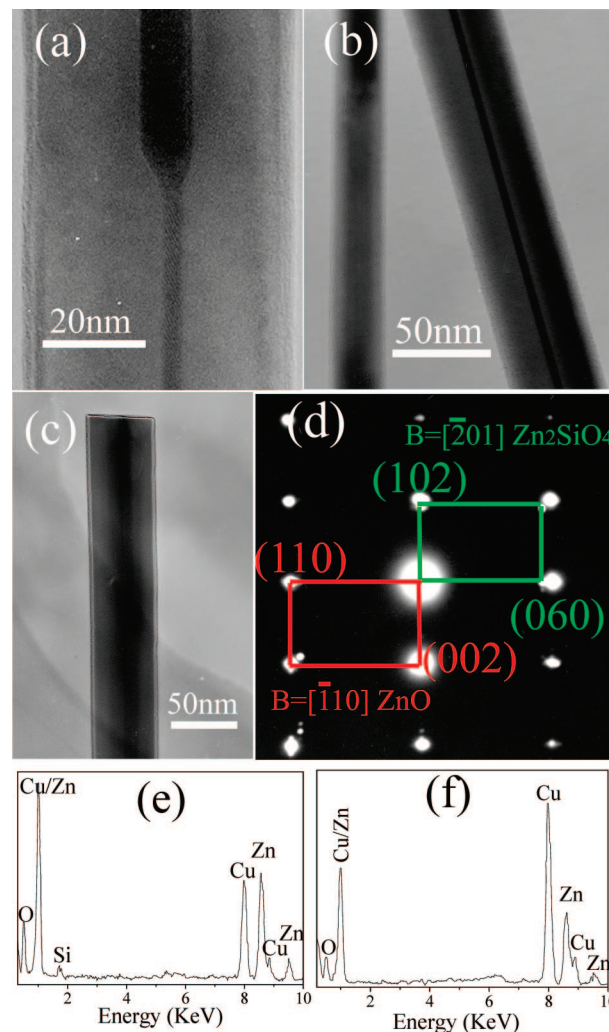

Figure 3. (a−c) Typical low-magnification TEM images showing uniform beltlike morphology with a dark core and bright edges. (d) The SAED pattern, showing a superposition of two specific patterns, and indexed to a hexagonal structured ZnO with [$\bar{1}$10] zone axis and an orthorhombic structured Zn$_2$SiO$_4$ with [$\bar{2}$01] zone axis. (e and f) EDS patterns, taken from the core and the edge of a relative broad nanobelt, respectively.

perpendicular to the surface of the nanobelt, indicates a superposition of two sets of single-crystal diffraction spots, which are indexed to be [$\bar{1}$10] ZnO and [$\bar{2}$01] Zn$_2$SiO$_4$ with an epitaxial orientation. EDS compositional analysis was performed in situ in TEM across a relatively broad nanobelt to investigate Si distribution. As shown in Figure 3, besides the Cu and C peaks from the carbon-coated TEM grid, Zn and O peaks are present in the spectrum. Furthermore, the Si signal in the spectra taken from the core is more evident than that from the two sides of the nanobelts, which further implies that the dark core is composed of Zn$_2$SiO$_4$

Two types of ZnO/Zn$_2$SiO$_4$ interfaces are observed in the core/shell heterostructure nanobelts. High-resolution TEM (HR-TEM) images in Figure 4 reveal an epitaxial relationship (002)$_{ZnO}$||(102)$_{Zn_2SiO_4}$ and [$\bar{1}$10]$_{ZnO}$||[$\bar{2}$01]$_{Zn_2SiO_4}$. Structurally, ZnO has a hexagonal crystal structure with lattice constants a = 0.3249 nm and c = 0.5206 nm (JCPDS 36-1451), and Zn$_2$SiO$_4$ has an orthorhombic crystal structure with lattice constants a = 0.9085 nm, b = 1.062 nm, and c = 0.5962 nm (JCPDS 40-0007). Thus, the mismatch between (002)$_{ZnO}$ and (102)$_{Zn_2SiO_4}$ is 8.45% (in reference to Zn$_2$SiO$_4$). The interference between the Bragg reflections from the two crystals
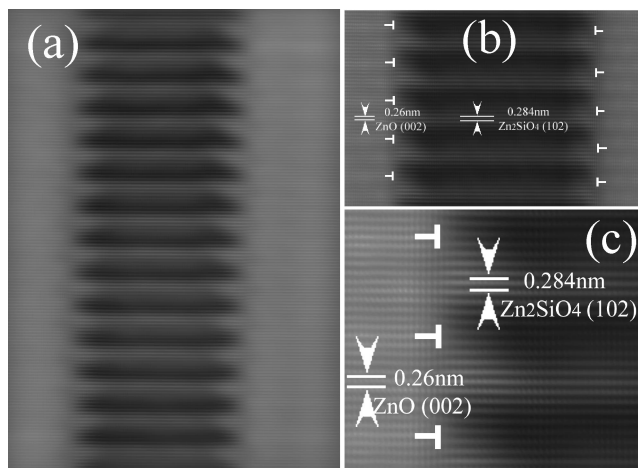
Figure 4. (a) HRTEM image, showing clear Moiré fringes in the dark core. (b and c) HRTEM images at higher magnification, showing that the semicoherent relation on the boundary and the period misfit dislocations (marked by T) can be clearly seen in the parallel interface.
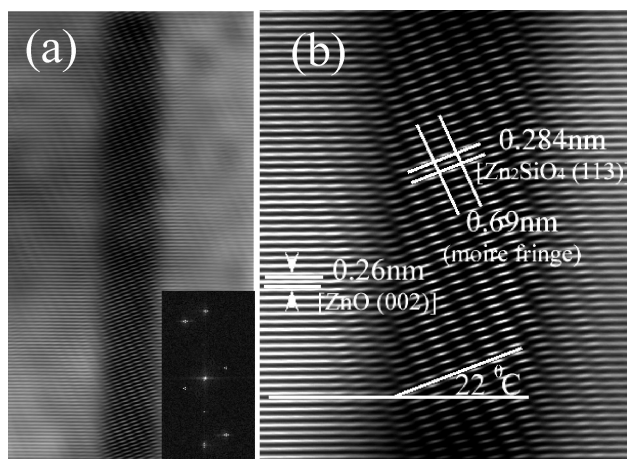

Figure 5. (a) HRTEM image and the corresponding FFT pattern (inset), showing a distinct difference of the contrast and the stripe between the core and the sheath. (b) Enlarged HRTEM image showing that (002) ZnO planes (shell) clockwise rotated 22° with respect to $(102)_{Zn_2SiO_4}$ planes (core) and then forming an inclined dislocation-free interface.
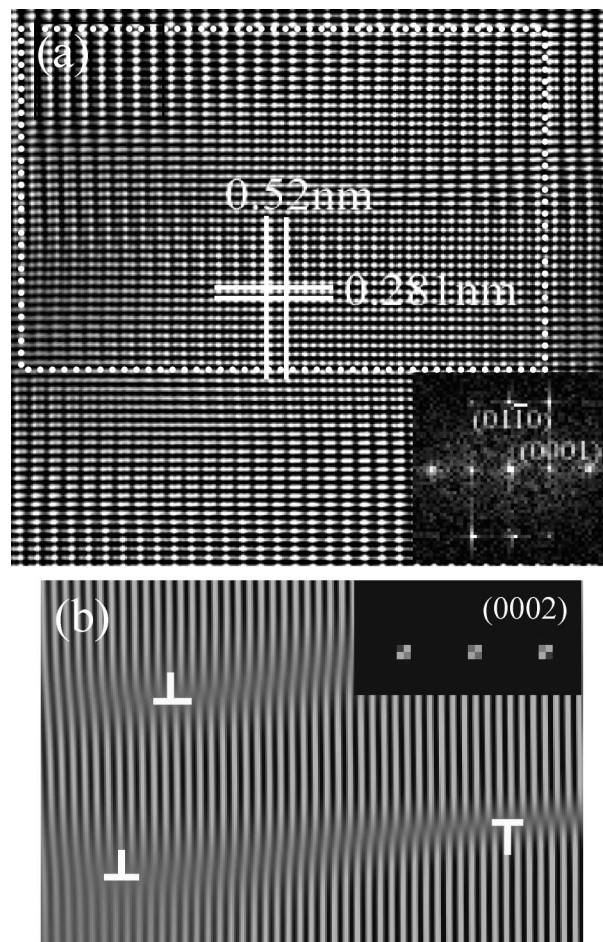

Figure 6. (a) HRTEM image of ZnO nanostructures taken at the [100] zone axis. (b) Back and forth FFT from ±(002) diffraction spots of the rectangle region bracketed in part a; dislocations are marked by "T", showing widely separated pairs of dislocations within the (001) planes.

produces ordered Moiré fringes solved by using the Moiré fringe images formed by two overlapping parallel planes or by two overlapping planes rotated with each other by an angle, which are apparent in the HRTEM image presented in Figures 4 and 5 at the core region where ZnO and Zn_2SiO_4 overlaps. The spacing of the Moiré fringes is given by

$$D = \frac{d_1 d_2}{\sqrt{d_1^2 + d_2^2 - 2d_1 d_2 \cos \theta}}$$

where d_1 and d_2 are the corresponding d spacings of the overlapping planes of the epitalayer and the substrate, and θ is the angle between d_1 and d_2.[9] Applying this equation for $d_1 = 0.284$ nm $[(102)_{Zn_2SiO_4}]$, $d_2 = 0.26$ nm $[(002)_{ZnO}]$, and $\theta = 0$, it can be found that $D = 3.124$ nm, which corresponds to one Moiré fringe every 11 atomic planes of Zn_2SiO_4 or 12 atomic planes of ZnO. Similarly, a periodicity array of edge dislocations is introduced in the parallel interface every 12 atomic planes of $(002)_{ZnO}$ or 11 atomic planes of $(102)_{SiO_4}$ due to interface mismatch, clearly shown in HRTEM images of Figure 4. To reduce interfacial stress, $(002)_{ZnO}$ planes tend to incline 22° with

respect to $(102)_{Zn_2}SiO_4$ planes and form a high-quality epitaxy without interface mismatch dislocations. The Moiré fringe spacing becomes 0.69 nm and its corresponding HRTEM images is present in Figure 5. The ZnO lattice stripe image in the shell regions, taken from the [100] zone axis, is further shown in Figure 6a and the image of the rectangle region bracketed is analyzed by the back and forth fast Fourier transformation (FFT) using only the ±(002) diffraction spots as shown in Figure 6b. Numerous opposite dislocation pairs denoted by "T", attributable to the substitution of different radius Si cations into the Zn sites in ZnO lattice,[10] are clearly observed. Thus, the stress can be partially relaxed through the formation of dislocations and lattice deformation throughout the ZnO nanobelts.

At the early stages of the thermal evaporation, quantities of Si−O vapor can sublimate from Si powder and quickly form Zn_2SiO_4 with ZnS vapor due to a relatively high content of residual O_2 in the ceramic tube. Since O_2 only comes from the leakage of the system, its content will decrease rapidly with prolongation reaction, and retain a certain level eventually. Furthermore, O could more readily react with ZnS than Si due to a large electronegativity of Si (1.9) relative to Zn (1.65). With the prolongation of thermal evaporation, therefore, the Si−O is insufficient for the creation of the Zn_2SiO_4 phase and is only incorporated into the ZnO lattice. As a result, the Si-doped ZnO shell can form on the surface of the initially formed Zn_2SiO_4 nanostructures by a certain epitaxy relationship.

Zn$_2$SiO$_4$/ZnO Core/Shell Coaxial Heterostructure Nanobelts

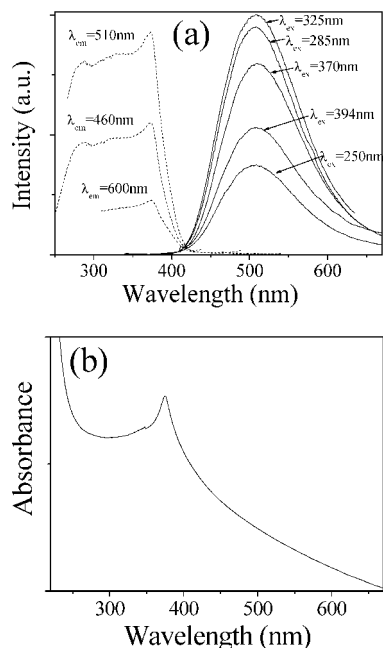*J. Phys. Chem. C, Vol. 112, No. 42, 2008* **16315**

Figure 7. (a) Room temperature PL (solid lines) and PLE (dash lines) spectra, taken under different wavelengths with a Xe pump as a light source. (b) UV−vis absorption spectrum.

The photoluminescence (PL; solid lines) and PL excitation (PLE; dash line) spectra, taken under various wavelengths with a xenon lamp as a light source, are shown in Figure 7. As can be seen from the emission spectra, an intense broadband emission, independent of excitation wavelength and centered at about 505 nm (2.45 eV), can be clearly observed. Similarly, the shape of excitation spectra is independent of monitored wavelengths, and furthermore, clearly visible excitonic transition peaks centered at about 373 nm can be observed in PLE spectra. The room temperature optical absorption spectrum is also shown in Figure 7b, which similarly exhibits a very sharp absorption peak at 375 nm near the absorption edge, close to the position of the excitonic absorption peaks in PLE spectra. The Bohr radius of ZnO has been estimated to be as small as 1.4 nm.[11] Excitonic localization easily occurs for small Bohr radius materials.[12] Furthermore, Si atoms are randomly distributed in the ZnO lattice and the presence of amounts of dislocations and interfacial states on the basis of the HRTEM analysis. Hence excitons are more readily localized by composition and defect fluctuations, resulting in the existence of a strong excitonic transition in doping nanostructures via optical absorption and excitation measurements.

For ZnO, generally, it not only has a deep level emission in the visible region due to structural defects and impurities, but it emits a near-UV light associated with the near-band-edge (NBE). To provide more information for understanding the nature of these transitions, excitation power-dependent room temperature PL measurements, which have been widely used for determining the origin of light emission in semiconductors, have been performed by the 325 nm line of a He−Cd laser and the result is given in Figure 8a. The two separated peaks can be clearly seen in the violet and green region of the PL spectra. For the NBE transition of the as-synthesized nanostructures, a large Stokes shift is observed with respect to the excitonic absorption peak (Figure 7). Furthermore, the peak position shows a larger red-shift with an increase in excitation density *I*, changing from 384.6 to 416.1 nm with increasing excitation density in the range of 0.2 to 20 kw/cm^2 and following the linear
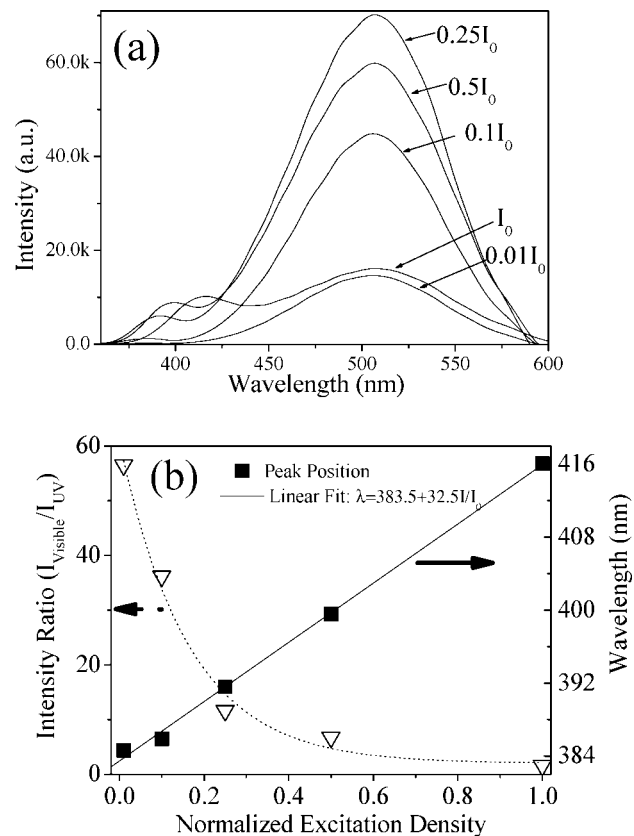

Figure 8. (a) Room temperature PL spectra of the sample at different excitation densities at constant radiation area (I_0 is the maximum value, about 20 kW/cm^2). (b) The peak position (solid square) of NBE violet emission and the integrated intensity ratio (hollow triangle) of the deep-level green emission to the NBE violet emission as a function of the excitation power intensity; the curves present corresponding fits.

relation $\lambda = 383.5 + 32.5I/I_0$ nm (solid line in Figure 8b) within our experimental range, where I_0 is about 20 kw/cm^2. At higher excitation, in addition, the NBE emission peak also shows a broader and more asymmetric line shape at its lower energy side. For the green emission, peaking at around 505 nm, their positions are independent of the excitation intensity, while their intensities show nonmonotonic dependence on the excitation density, as illustrated in Figure 8a. The intensity increases initially, passes through a maximum at $0.25I_0$ excitation intensity, and then decreases gradually with further increasing excitation intensity. It is more interesting that the ratio in integrated PL intensity of the green emission to the NBE luminescence decreases monotonously with the excitation density as indicated by the dotted line in Figure 8b.

Upon photoexcitation of a semiconductor particle an electron−hole pair, existing as a Wannier exciton, is created and recombines radiatively a photon with energy close to its band gap. The electron and/or the hole from a Wannier exciton can be trapped in shallow levels or in deep traps in the particle.[13] In our sample, amounts of dislocations and interfacial states, induced by the impurities, form a defect complex with intrinsic defect (likely oxygen vacancies V$_O$), acting as a deep trap, and capture holes. Its energetic position is almost invariant with excitation wavelength and intensity and only determined by the chemical nature of the trap and by the local structure surrounding the trapped charge carriers. Furthermore, the rate of this hole trapping is much faster than that of the exciton radiative recombination.[13] Thus, efficient and fast trapping of photogenerated holes in these

defect complexes can be expected. At low excitation intensity, such as a Xe lamp, photogenerated electrons with a relatively low density more readily transfer from a shallow level close to the conduction band edge to the deeply trapped hole and emit a visible light with 2.45 eV photons, referred to trap emission. As the sample is excited by a He−Cd laser with a relatively high power density, amounts of electrons are excited to the conduction band, and furthermore, partial photogenerated holes can also be captured by shallow levels due to the saturation of deep trap states. Hence, the exciton-related NBE emission can also emerge under excitation with a He−Cd laser. The energetic position of a shallow trap depends strongly on the band structure of the material.[14] As the excitation intensity further increases, much higher density of charge carriers induces many body effects, resulting in bandgap renormalization and shrinkage.[15] Additionally, impurity and defect inhomogeneities can induce band tail localization.[16] Thus, the violet emission is mainly governed by the direct transition of photogenerated electrons to the valence band tail states, referred to as the transition of free electrons to free holes, and exhibits a power-dependent red-shift. Furthermore, the low-energy side of NBE emission shows a broader and more asymmetric tail with increasing excitation intensity. At higher excitation density, thermal energy can induce structure relaxation and strain release, resulting in a delocalization of holes in deep trap sites. For the NBE and the trap emission, moreover, the two processes are in competition with each other. Therefore, amounts of free electrons will recombine directly with free holes. As a consequence, the trap-related emission increases up to a maximum at $0.25I_0$ excitation intensity and thereafter decreases, and the emission intensity ratio of the NBE to the trap states increases monotonously with increasing excitation intensity. Due to the spatial localization of deep trapped states, the position of green emission is independent of the excitation wavelength and intensity. It is also well-known that Zn_2SiO_4, whose optical bandgap is reported to be about 5.5 eV, is also a green luminescent material.[17] As a result, the two green bands could be easily overlapped while ZnO and Zn_2SiO_4 coexist in the nanostructures, further resulting in a very strong green emission.

4. Conclusions

In summary, Zn_2SiO_4/ZnO core/shell radial heterostructure nanobelts with an epitaxial orientation relationship were synthesized by a vapor-transport-deposition method due to a change in the O_2 concentration during the growth. Due to the lattice mismatch, a parallel interface with a periodicity array of edge dislocations and an inclined interface without dislocations can be formed. Ordered Moiré interference fringes can be observed in the core due to the epitaxial overlap of ZnO on Zn_2SiO_4 crystals, and furthermore, amounts of disordered dislocations also exist in ZnO lattice due to the incorporation of Si. It is due to fluctuation of Si composition and defect, carrier localization by deep traps from defect and impurity complex, and variation in free-carrier concentration that the optical properties of doping samples are greatly influenced. A strong excitonic transition exhibits in optical absorption and excitation spectra due to excitonic localization from a spatial fluctuation of Si content in the nanostructures. Due to band tail localization, and the increase of free-carriers induced by the doping, especially the dissociation of the bound excitons with increasing excitation intensity, the NBE emission is dominated by the

transition of free-electrons to free-holes, and furthermore shows characteristics of an excitation power-dependent red-shift and a broader and more asymmetric tail at its low energy edge. The high density of deep traps related to the complex of impurities and defects makes the green emission predominant in PL spectra. At higher excitation intensity, furthermore, the thermalization effect induces the structure relaxation and the strain release, resulting in the delocalization of free carriers in deep traps. As a consequence, the green emission passes through a maximum at $0.25I_0$ excitation intensity, and the violet-to-green emission intensity ratio increases monotonously with increase in excitation density. These unique properties suggest that the violet and green emission of ZnO nanostructures can be well tuned by a moderate doping and a variation in the excitation density.

References and Notes

(1) (a) Harada, Y.; Hashimoto, S. *Phys. Rev. B* **2003**, *68*, 045421. (b) Wu, X. L.; Siu, G. G.; Fu, C. L.; Ong, H. C. *Appl. Phys. Lett.* **2001**, *78*, 2285. (c) Pearton, S. J.; Norton, D. P.; Ip, K.; Heo, Y. W.; Steiner, T. *Superlattices Microstruct.* **2003**, *34*, 3.

(2) (a) Huang, M. H.; Mao, S.; Feick, H.; Yan, H.; Wu, Y.; Kind, H.; Weber, E.; Russo, R.; Yang, P. D. *Science* **2001**, *292*, 1897. (b) Hughes, W. L.; Wang, Z. L. *Appl. Phys. Lett.* **2003**, *82*, 2886. (c) Bai, X. D.; Wang, E. G.; Bai, P. X.; Wang, Z. L. *Appl. Phys. Lett.* **2003**, *82*, 4806. (d) Qin, Y.; Wang, X. D.; Wang, Z. L. *Nature* **2008**, *451*, 809.

(3) (a) Tian, Z. R. R.; Voigt, J. A.; Liu, J.; Mckenzie, B.; Mcdermott, M. J. *J. Am. Chem. Soc.* **2002**, *124*, 12954. (b) Tian, Z. R. R.; Voigt, J. A.; Liu, J.; McKenzie, B.; McDermott, M. J.; Rodriguez, M. A.; Konishi, H.; Xu, H. F. *Nat. Mater.* **2003**, *2*, 821. (c) Zhao, F. H.; Li, X. Y.; Zheng, J. G.; Yang, X. F.; Zhao, F. L.; Wong, K. S.; Wang, J.; Lin, W. J.; Wu, M. M.; Su, Q. *Chem. Mater.* **2008**, *20*, 1197. (d) Yu, Q. J.; Fu, W. Y.; Yu, C. L.; Yang, H. B.; Wei, R. H.; Li, M. H.; Liu, S. K.; Sui, Y. M.; Liu, Z. L.; Yuan, M. X.; Zou, G. T. *J. Phys. Chem. C* **2007**, *111*, 17521. (e) Sounart, T. L.; Liu, J.; Voigt, J. A.; Hsu, J. W. P.; Spoerke, E. D.; Tian, Z.; Jiang, Y. B. *Adv. Funct. Mater.* **2006**, *16*, 335.

(4) (a) Yuhas, B. D.; Zitoun, D. O.; Pauzauskie, P. J.; He, R. H.; Yang, P. D. *Chem. Int. Ed.* **2006**, *45*, 420. (b) Cui, J. B.; Soo, Y. C.; Chen, T. P.; Gibson, U. J. *J. Phys. Chem. C* **2008**, *112*, 4475. (c) Bhattacharyya, S.; Gedanken, A. *J. Phys. Chem. C* **2008**, *112*, 4517. (d) Hao, Y. F.; Meng, G. W.; Wang, Z. L.; Ye, C. H.; Zhang, L. D. *Nano Lett.* **2006**, *6*, 1650. (e) Rakshit, S.; Vasudevan, S. *J. Phys. Chem. C* **2008**, *112*, 4531.

(5) (a) Zou, K.; Qi, X. Y.; Duan, X. F.; Zhou, S. M.; Zhang, X. H. *Appl. Phys. Lett.* **2005**, *86*, 013103. (b) Cheng, B. C.; Wang, Z. G. *Adv. Funct. Mater.* **2005**, *15*, 1883. (c) Cheng, B. C.; Xiao, Y. H.; Wu, G. S.; Zhang, L. D. *Adv. Funct. Mater.* **2004**, *4*, 913. (d) Hao, Y. F.; Meng, G. W.; Ye, C. H.; Zhang, L. D. *Appl. Phys. Lett.* **2005**, *87*, 033106. (e) Lommens, P.; Loncke, F.; Smet, P. F.; Callens, F.; Poelman, D.; Vrielinck, H.; Hens, Z. *Chem. Mater.* **2007**, *19*, 5576.

(6) (a) Song, J.; Wang, X.; Riedo, E.; Wang, Z. L. *J. Phys. Chem. B* **2005**, *109*, 9869. (b) Park, J. H.; Choi, Y. J.; Park, J. G. *J. Cryst. Growth* **2005**, *280*, 161.

(7) (a) Seo, H. W.; Bae, S. Y.; Park, J. *Appl. Phys. Lett.* **2003**, *82*, 3752. (b) Qi, H.; Wang, C.; Liu, J. *Adv. Mater.* **2003**, *15*, 411. (c) Wen, B. M.; Huang, Y. Z.; Boland, J. J. *J. Phys. Chem. C* **2008**, *112*, 106. (d) Zhang, Z.; Wang, S. J.; Yu, T.; Wu, T. *J. Phys. Chem. C* **2007**, *111*, 17500.

(8) (a) Fan, D. H.; Ning, Z. Y.; Jiang, M. F. *Appl. Surf. Sci.* **2004**, *245*, 414. (b) Zheng, T. H.; Li, Z. Q.; Chen, J. K.; Shen, K.; Sun, K. F. *Appl. Surf. Sci.* **2006**, *252*, 8482.

(9) (a) Yang, P. D.; Yan, H.; Mao, S.; Russo, R.; Johnson, J.; Saykally, R.; Morris, N.; Pham, J.; He, R.; Choi, H. J. *Adv. Funct. Mater.* **2002**, *12*, 323. (b) Lyu, S. C.; Zhang, Y.; Lee, C. J.; Ruh, H.; Lee, H. J. *Chem. Mater.* **2003**, *15*, 3294.

(10) (a) Ronning, C.; Gao, P. X.; Ding, Y.; Wang, Z. L.; Schwen, D. *Appl. Phys. Lett.* **2004**, *84*, 783. (b) Yang, Y.; Sun, X. W.; Tay, B. K.; Cao, P. H. T.; Wang, J. X.; Zhang, X. H. *J. Appl. Phys.* **2008**, *103*, 064307.

(11) Thomas, D. G. *J. Phys. Chem. Solids* **1960**, *15*, 86.

(12) Tampo, H.; Shibata, H.; Maejima, K.; Yamada, A.; Matsubara, K.; Fons, P.; Niki, S.; Tainaka, T.; Chiba, Y.; Kanie, H. *Appl. Phys. Lett.* **2007**, *91*, 261907.

(13) Van Dijken, A.; Meulenkamp, E. A.; Vanmaekelbergh, D.; Meijerink, A. *J. Phys. Chem. B* **2000**, *104*, 1715.

(14) Brus, L. *J. Phys. Chem.* **1986**, *90*, 2555.

Zn$_2$SiO$_4$/ZnO Core/Shell Coaxial Heterostructure Nanobelts

J. Phys. Chem. C, Vol. 112, No. 42, 2008 **16317**

(15) Yoo, Y. Z.; Jin, Z. W.; Chikyow, T.; Fukumura, T.; Kawasaki, M.; Koinuma, H. *Appl. Phys. Lett.* **2002**, *81*, 3798.

(16) (a) Polimeni, A.; Masia, F.; Vinattieri, A.; Baldassarri Höger von Högersthal, G.; Capizzi, M. *Appl. Phys. Lett.* **2004**, *84*, 2295. (b) Buyanova, I. A.; Bergman, J. P.; Pozina, G.; Chen, W. M.; Rawal, S.; Norton, D. P.; Pearton, S. J.; Osinsky, A.; Dong, J. W. *Appl. Phys. Lett.* **2007**, *90*, 261907. (c) AÏt-Ouali, A.; Yip, R. Y. F.; Brebner, R. A. *J. Appl. Phys.* **1998**, *83*, 3153.

(17) (a) Sohn, K. S.; Cho, B.; Park, H. D. *J. Am. Ceram. Soc.* **1999**, *82*, 2779. (b) Xu, X. L.; Guo, C.; Qi, Z.; Liu, H. T.; Xu, J.; Shi, C. S.; Chong, C.; Huang, W. H.; Zhou, Y. J.; Xu, C. M. *Chem. Phys. Lett.* **2002**, *364*, 57. (c) Wang, X. D.; Summers, C. J.; Wang, Z. L. *Adv. Mater.* **2004**, *16*, 1215. (d) Zhou, J.; Liu, J.; Wang, X. D.; Song, J. H.; Tummala, R.; Xu, N. S.; Wang, Z. L. *Small* **2007**, *3*, 622.